

## Finite-size versus periodic effects in Ni/Co multilayers

L. Chico,<sup>1</sup> M. P. López-Sancho,<sup>2</sup> and M. C. Muñoz<sup>2</sup>

<sup>1</sup>*Departamento de Física Aplicada, Facultad de Ciencias del Medio Ambiente, Universidad de Castilla-La Mancha, 45071 Toledo, Spain*

<sup>2</sup>*Instituto de Ciencia de Materiales de Madrid, Consejo Superior de Investigaciones Científicas, Cantoblanco, 28049 Madrid, Spain*

(Received 17 April 2001; revised manuscript received 8 November 2001; published 7 May 2002)

The periodic effects on the electronic properties of Ni/Co magnetic multilayers grown in the (111) direction are investigated by studying superlattices and finite bilayers formed with the same unit block. Band structures and Fermi surfaces are calculated using a Green-function-matching method within a self-consistent empirical tight-binding model. Our results show strong *sp-d* hybridization of the electronic levels, the existence of nested multisheet Fermi surfaces, and the occurrence of *d*-derived spatially extended states in both superlattices and finite bilayers. Nevertheless, the superlattice periodicity increases the band degeneracy in the in-plane direction and changes the energy position of the superlattice electron levels with respect to those of the bilayer. The discrepancies result in different Fermi wave vectors for both systems, which may yield different transport and dynamical coupling characteristics for superlattices and bilayers.

DOI: 10.1103/PhysRevB.65.184429

PACS number(s): 75.70.Cn, 71.18.+y, 71.20.Be

### I. INTRODUCTION

Magnetic and transport properties of multilayers (ML) are one of the main focus of research on metallic mesoscopic systems, because there are striking differences between the properties of multilayers (ML's) and those corresponding to the constituent metals. Under the generic name of ML's there are included a great variety of layered structures ranging from a single bilayer (BL), formed by two coupled slabs of different metals, to a superlattice (SL), in which the bilayer unit block is repeated periodically. Between these two extremes there are numerous and different finite-size structures. Although distinct ML phenomena, as oscillatory exchange coupling and giant magnetoresistance (GMR), are observed in all kinds of ML's, there are peculiar characteristics that can be ascribed to a particular type of ML. Perpendicular magnetic anisotropy has been observed in a great variety of layered heterostructures. In particular, on the basis of *ab initio* calculations it was predicted and experimentally verified<sup>1</sup> that the presence of an interface between ultrathin close-packed layers of Co and Ni is sufficient to give rise to a large perpendicular magnetic anisotropy. Ni/Co heterostructures have an added interest due to the magnetic character of both constituent materials and lately they have attracted much attention. X-ray absorption experiments show<sup>2</sup> that the density of *3d* holes increases almost by 20% from submonolayer to five-monolayer-thick films of Ni grown on Cu(001). Moreover, an enhancement of the spin and orbital magnetic moments of two-monolayer Co thin films on Cu(001) were determined by x-ray magnetic circular dichroism,<sup>3</sup> while both spin and orbital moments of four-monolayer Ni films on Cu(001) were reduced. Furthermore, during the initial stages of interface formation of ferromagnetic Ni films grown epitaxially on ultrathin films of Co the Ni spin moment decreases and the Co spin moment increases.<sup>4</sup> This effect is explained in terms of a modified exchange splitting arising from the charge redistribution between *d* states.<sup>5</sup> However, the observed variations of the spin moments contradict the results of recent first-principles band-structure calculations

for the Ni/Co interface.<sup>6,7</sup> The discrepancy between theoretical predictions and experimental findings may be due to the difficulty in calculating a spin-dependent exchange and correlation energy at the interface of two ferromagnetic materials, since calculations for the Ni/Cu and Co/Cu interfaces have proven to be highly accurate.<sup>6,8</sup> Therefore, the interface magnetism of Ni-Co remains an open question and probably calculations beyond the one-electron approximation need to be performed.

The dependence of the GMR on the number of bilayer repeats in Co/Cu(001) ML has also been investigated starting from spin-density functional theory, where the in-plane transport is calculated quasiclassically by solving the linearized Boltzmann equation in the relaxation time approximation.<sup>9</sup> The study concludes that the GMR ratio as a function of the bilayer repeat increases and reaches saturation for more than 10 BL's; the dependence was attributed not to intrinsic finite-size effects but to diffusive surface scattering. The present work is motivated by the experimental evidence that the SL transport coefficients behave differently from those of a single bilayer. In fact, the low-temperature resistivity, anisotropic magnetoresistance, and anomalous Hall coefficient of Ni/Co(111) SL's oscillate as a function of layer thicknesses. The oscillatory behavior was shown to be a SL effect, since the oscillation disappears when the number of periods in the SL decreases.<sup>10</sup> Furthermore, based on a simplified model the oscillation has been associated with periodic changes in the density of states at the Fermi level,<sup>11</sup> although a more complex semiempirical calculation does not account for the oscillation.<sup>12</sup> Nevertheless, conductance calculations of a finite SL connected to pure crystalline semi-infinite leads predict oscillations of the conductance as a function of both magnetic and spacer layer thickness, although their magnitude is much smaller than those observed experimentally.<sup>13</sup>

On the other hand, theoretical calculations in a model system of the interlayer exchange coupling in finite magnetic trilayers show new features of the interlayer coupling phenomena.<sup>14</sup> A nonsinusoidal oscillatory behavior of the coupling with both magnetic and spacer layer thicknesses

has been obtained in both symmetric and asymmetric trilayers. Moreover, for asymmetric trilayers in which the thicknesses of the magnetic slabs are different, the dependence of the coupling constant on the thickness of a magnetic layer shows a peculiar behavior. Their magnitude does not decay monotonically; instead, it is modulated by a sinusoidal function.<sup>15</sup> Nevertheless, interlayer exchange coupling calculations predict the same oscillations period for both Co/Cu and Ni/Cu(100) SL's and BL's.<sup>16</sup> These results raise questions about superlattice effects in ML's. In this article we address the finite-size dependence of the electronic properties of Ni/Co ML's by studying a single bilayer, formed by two coupled slabs, one of Ni and one of Co, grown in the (111) direction, compared to the corresponding SL constructed by a periodic repetition of the bilayer unit block. We focus on the similarities and differences of the electron density distribution. The differences arising between both structures are due only to the SL periodicity, since quantum-size effects produced by the finite size of the constituent Co and Ni slabs, as well as partial electron reflection and transmission at the Ni/Co interface, will occur in both SL and BL and are treated exactly in the Green function matching approach used in the calculation. The method is particularly appropriate for treating systems without translational symmetry, since it does not introduce any artificial supercell or superperiodicity.

## II. MODEL AND METHOD

The  $\text{Ni}_n\text{Co}_m$  BL and SL structures investigated differ by their dimensionality. While the BL's are quasi-two dimensional, the SL's are actual three-dimensional (3D) systems with a superperiodicity—superimposed on that of the perfect fcc crystal—given by the number of  $n+m$  layers forming the SL unit block. Therefore, the SL Hamiltonian has translational invariance, and continuous states and electronic bands develop in all directions. On the other hand, the finite size of the BL causes discrete localized electronic levels, since the electron motion in the BL growth direction becomes quantized.  $\text{Ni}_n\text{Co}_m$  SL's belong to two different space groups, hexagonal if  $n+m$  is a multiple of three and trigonal otherwise,<sup>17</sup> while the BL symmetry corresponds to the two-dimensional (2D) hexagonal groups, independently of the number of layers. Moreover, although the potential discontinuity at the Ni/Co interface is the same in both structures, the

complete potential profiles are different for BL's and SL's. In the SL it is symmetric and periodic, while in the BL it is asymmetric and coupled to the vacuum through the surface potential at the extreme layers. This results in different boundary conditions, which gives rise to different electronic spectra.

Ni/Co heterostructures—both SL's and BL's—have been epitaxially grown in the fcc structure along the (111) direction.<sup>10,11</sup> They present very sharp interfaces, so we study ideal layered structures with perfect interfaces. The electronic properties are calculated using a Green-function-matching (GFM) method within a self-consistent empirical tight-binding model.<sup>17,18</sup> Both the long-range structural coherence of SL and the limited size of BL are treated exactly in the GFM framework. The method combines elements of scattering theory with the treatment of the boundary conditions, and provides the formulas needed for actual calculations. To obtain the SL and BL Green functions (GF's), we follow the matching procedure developed in Ref. 18. All the matrix elements of the total GF's are obtained in terms of the Hamiltonians and GF's of the constituent metals and the coupling interactions across the interfaces. In Ref. 18 a complete derivation of all the superlattice GF matrix elements was given. For the bilayer a complete set of dual formulas can be obtained following an analogous procedure. We define  $P_A$  and  $P_B$  as the unit projectors spanning the complete  $A$ - and  $B$ -bounded slabs forming the BL structure.  $A_1, A_2, \dots, A_N$  and  $B_1, B_2, \dots, B_M$  denote the layers of the  $A$  and  $B$  slabs, respectively. The term layer indicates a *principal layer*, which by definition is coupled only to nearest-neighbor *principal layers* and may contain more than an atomic plane.<sup>18</sup> The fundamental characteristic of the GFM analysis is that all the matching features of any system with one or more interfaces are included in the *interface projection domain*, which in the BL structure includes four layers  $I = \{A_1, A_N, B_1, B_M\}$ :  $A_1$  and  $B_M$  are the two external layers at the BL-vacuum interface, whereas  $A_N$  and  $B_1$  layers form the actual interface between the  $A$  and  $B$  slabs. The full  $I$  domain can be decomposed into the  $I_A = \{A_1, A_N\}$  and  $I_B = \{B_1, B_M\}$  interface projectors. With these definitions and considering that all the bulk  $A$  and  $B$  operators are defined only in their own  $A$  or  $B$  space, the matching analysis yields for the BL Green function interface projection the following expression:

$$\tilde{G}_{\text{BL}}^{-1} = \begin{pmatrix} E - H_{A_1A_1} - D_{A_1A_1} & -D_{A_1A_N} & 0 & 0 \\ -D_{A_NA_1} & E - H_{A_NA_N} - D_{A_NA_N} & -H_{A_NB_1} & 0 \\ 0 & -H_{B_1A_N} & E - H_{B_1B_1} - D_{B_1B_1} & -D_{B_1B_M} \\ 0 & 0 & -D_{B_MB_1} & E - H_{B_MB_M} - D_{B_MB_M} \end{pmatrix}, \quad (1)$$

where

$$D_X = \begin{pmatrix} D_{X_1X_1} & D_{X_1X_l} \\ D_{X_lX_1} & D_{X_lX_l} \end{pmatrix} = \begin{pmatrix} H_{X_1X_2} & 0 \\ 0 & H_{X_lX_{l-1}} \end{pmatrix} \begin{pmatrix} T_X & \bar{T}_X^{l-2} \\ T_X^{l-2} & \bar{T}_X \end{pmatrix} \begin{pmatrix} 1 & \bar{T}_X^{l-1} \\ T_X^{l-1} & 1 \end{pmatrix}^{-1}. \quad (2)$$

In the previous formula  $X=A,B$  and  $l=N$  if  $X=A$  and  $l=M$  if  $X=B$ ;  $H_{X_n,X_m}$ , with  $X=A,B$ , are the Hamiltonian matrix elements between layers  $X_n$  and  $X_m$ ,  $H_{A_N,B_1}$  is the coupling interaction across the  $A$  and  $B$  interface, and  $T_X$  and  $\bar{T}_X$  are the transfer matrices that relate different elements of the bulk Green functions. They are defined as

$$G_{n+1,m} = TG_{n,m}, \quad n \geq m$$

$$G_{n-1,m} = \bar{T}G_{n,m}, \quad n \leq m.$$

The Hamiltonian and Green-function matrix elements are functions of the in-plane  $\mathbf{k}_{\parallel}$  vector, energy, and spatial coordinates in the growth direction, since the bilayer retains 2D periodicity. From  $\tilde{G}_{BL}$  the matrix elements of  $G_{BL}$  between any layers of the entire structure can be evaluated.<sup>18</sup>

The differences between the SL and BL Green functions arise from the differences between the SL and BL interface domain; while in the SL it involves two coupled interfaces, in the BL there is no direct coupling between the external boundaries of the two constituent Ni and Co slabs. This results in different expressions for the interface projected Green functions.

The basis used in all calculations is the spin-polarized *spd* layered-orbital set with the parameters reported in Ref. 17. They include up to second-nearest-neighbor interactions and are calculated self-consistently to fit *ab initio* self-consistent spin polarized Korringa-Kohn-Rostoker (KKR) band structures<sup>19,20</sup> and available experimental data.<sup>21,22</sup> The cross-coupling matrix elements were evaluated by a self-consistent procedure for a single Ni-Co interface. Energies throughout are relative to the Fermi energy ( $E_F$ ) and wave vectors are measured in units of the length of the special line to which they belong.

### III. RESULTS AND DISCUSSION

The electronic properties have been calculated for different SL periods and slab thicknesses. The general behavior and the calculated trends are similar; therefore we only show the results corresponding to  $\text{Ni}_4\text{Co}_4$ ,  $\text{Ni}_4\text{Co}_5$ , and  $\text{Ni}_5\text{Co}_4$  SL's and BL's. The  $\text{Ni}_4\text{Co}_5$  and  $\text{Ni}_5\text{Co}_4$  SL's have hexagonal symmetry, and then all the cross sections of the hexagonal 3D Brillouin zone (BZ) of the superlattice are equal to the hexagonal 2D BZ of the bilayer. On the other hand, the  $\text{Ni}_4\text{Co}_4$  SL belongs to the trigonal space group and only the  $k_z=1/2$  cross section and the boundary planes of the 3D BZ are regular hexagons. Figure 1 represents the near- $E_F$  spin-up dispersion relations for the  $\text{Ni}_4\text{Co}_5$  SL, along in-plane ( $\Gamma M$  and  $\Gamma K$ ) and perpendicular ( $\Gamma A$ ) high-symmetry lines of the hexagonal 3D BZ. In all directions, there are subbands with a major *sp*-like character, unequivocally distinguishable from those with a predominant *d*-like orbital component: while the former present a parabolic free-electron-like behavior the latter have very small energy dispersion. In the displayed interval almost all subbands cross in the three directions; the exceptions are the subbands lo-

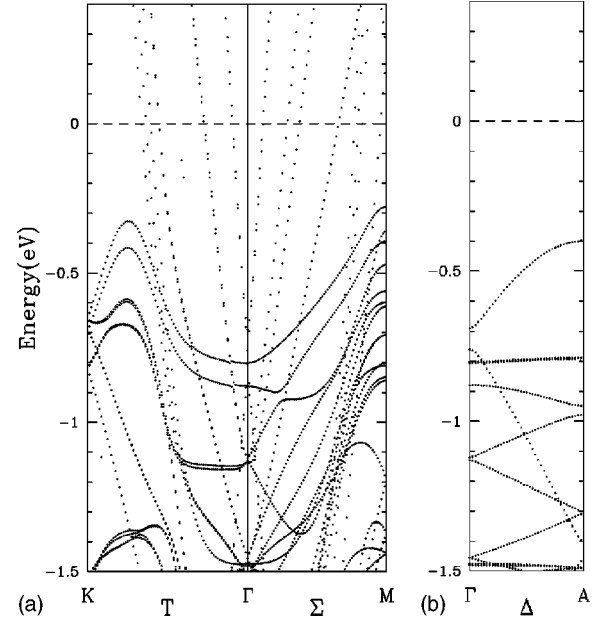


FIG. 1. Band structure of the  $\text{Ni}_4\text{Co}_5$  superlattice for spin-up polarized states along the high-symmetry directions of the BZ: (a) for the in-plane directions  $\Gamma K$  and  $\Gamma M$ ; (b) for the SL growth direction  $\Gamma A$ .

cated around  $-0.9$  eV at  $\Gamma$ , for which anticrossings occur in the  $T$  and  $\Sigma$  directions close to the  $\Gamma$  point. Crossings and anticrossings are allowed in these directions, since the factor groups  $C_{2v}$  and  $C_{6v}$ , corresponding to the in-plane and perpendicular directions, contain four one-dimensional and one and two twofold irreducible representations, respectively. All subbands crossing the Fermi level present the free-electron-like behavior characteristic of predominant *sp*-like character. In contrast, along  $\Delta$  most subbands have a mixed *sp-d* character, which is clearly evident in the dispersion relation: almost all subbands disperse as a function of  $k_z$  in spite of its predominant *d*-like orbital component. Band mixing is a manifestation of the strong *sp-d* hybridization occurring for spin-up electrons below the Fermi level. The electron mixing and a strong *sp-d* hybridization have been invoked to explain experimental measurements of the Ni/Co interface magnetism.<sup>4,5</sup> Moreover, along  $\Delta$  there is a large gap around  $E_F$  for spin-up electrons and the top of the valence band is at the  $A$  point of the SL BZ boundary plane. The dispersion relation along this direction clearly shows the zone-folded origin of the SL subbands, which correspond to a remapping of the original Ni and Co (111) fcc bulk band in the smaller SL BZ, with opening of gaps at the zone boundary. In fact, the top of the band in the  $\Gamma A$  direction has its origin in the  $L_2'$  Ni and Co bands.

Figure 2 shows the corresponding band structure for the 2D BZ of the  $\text{Ni}_4\text{Co}_5$  BL. The general features are similar to those found for the SL. However, there are two distinct characteristics: the number of bands and their relative positions are different from those of the SL. There are more bands and they are more uniformly distributed in the displayed energy

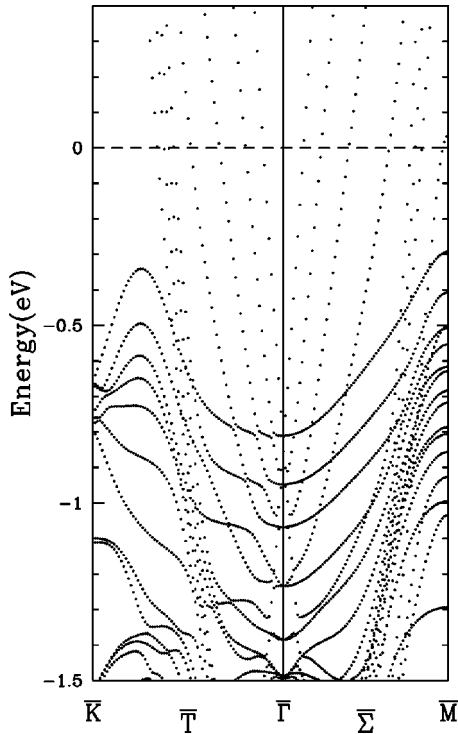


FIG. 2. Band structure of the  $\text{Ni}_4\text{Co}_5$  bilayer for spin-up polarized states along the high-symmetry directions  $\bar{\Gamma}K$  and  $\bar{\Gamma}M$  of the two-dimensional BZ.

interval. In fact, numerous SL degenerate bands are separated in the BL. The breaking of symmetry is specially significant in the  $\bar{T}$  direction. Besides, most split bands anticross with the quasi-free-electron subbands. The new anticrossings, due to the allowed interactions among BL states, are not present in the SL dispersion relation along  $T$  (see Fig. 1). The increase in the number of BL subbands obviously corresponds to a larger number of peaks in the density of states for a given wave vector; this is clearly observed in Fig. 3, which shows the local density of states (LDOS) as a function of energy at  $k \approx 0.8$  in the  $T$  and  $\bar{T}$  directions for the  $\text{Ni}_4\text{Co}_5$  SL and BL, respectively.

The discrepancies between the SL and BL electronic structures are not exclusive of ML's with hexagonal symmetry. In fact, the  $\text{Ni}_4\text{Co}_4$  SL, which belongs to the trigonal group, shows an analogous behavior. Figures 4 and 5 represent the SL and BL dispersion relations. The general features are equivalent to those shown by  $\text{Ni}_4\text{Co}_5$  ML's, although there are fewer subbands due to the decrease in the total number of layers. The lowering of symmetry associated with finite-size effects are similar for SL's with hexagonal or trigonal symmetry. Nonetheless, there is a significant difference between the  $\text{Ni}_4\text{Co}_4$  and the  $\text{Ni}_4\text{Co}_5$  SL dispersion relations. Although the top of the band in the perpendicular  $\bar{\Gamma}Z$  and  $\bar{\Gamma}A$  directions is almost at the same energy (approximately 0.4 eV below the Fermi level), it is located at different  $k$  points; i.e., the zone center  $\bar{\Gamma}$  for the  $\text{Ni}_4\text{Co}_4$  and the zone boundary  $A$  for the  $\text{Ni}_4\text{Co}_5$  SL. This is a direct consequence of the zone-folding effects governing the SL band structures. The differences in  $k$  space are not characteristic of

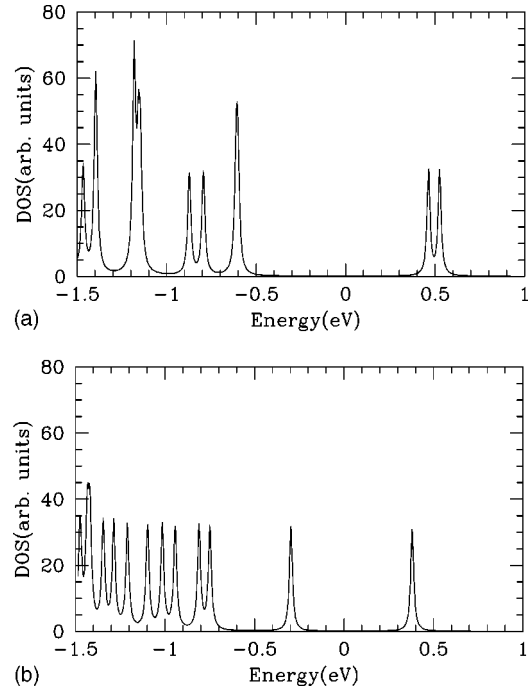


FIG. 3. Spin-up polarized local DOS as a function of the energy at  $k \approx 0.8$  in the in-plane  $T$  (and  $\bar{T}$ ) direction: (a) for the  $\text{Ni}_4\text{Co}_5$  SL; (b) for the  $\text{Ni}_4\text{Co}_5$  BL.

these particular SL's, but it is always present in SL's with periods differing in an odd number of atomic layers. However, the energy differences decrease as the number of layers increase, so it is more important for small-period SL's. The energy position of the highest level at the  $\bar{\Gamma}$  point, which corresponds to the mentioned SL's is almost the same in both

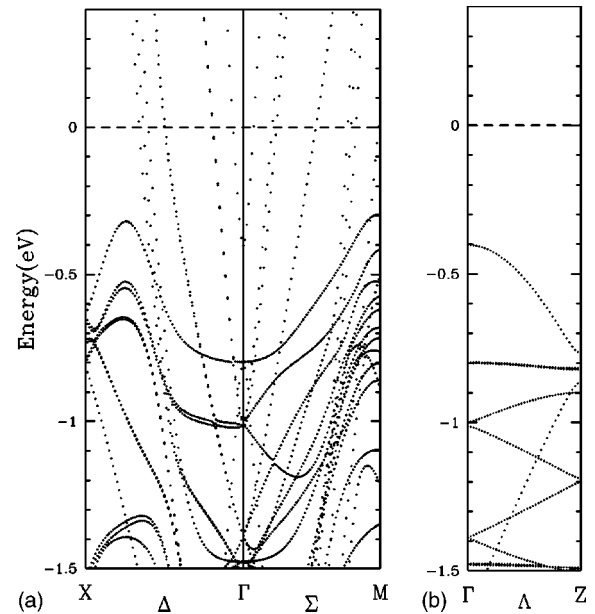


FIG. 4. Band structure of the  $\text{Ni}_4\text{Co}_4$  superlattice for spin-up polarized states along the high-symmetry directions of the BZ: (a) for the in-plane directions  $\bar{\Gamma}X$  and  $\bar{\Gamma}M$ ; (b) for the SL growth direction  $\bar{\Gamma}Z$ .

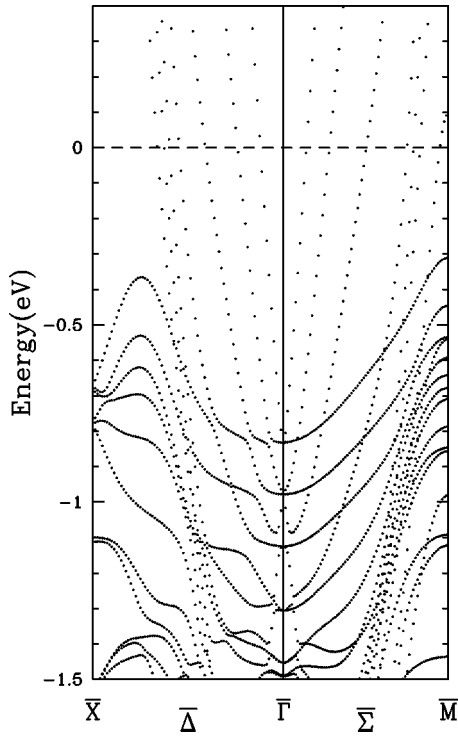


FIG. 5. Band structure of the  $\text{Ni}_4\text{Co}_4$  bilayer for spin-up polarized states along the high-symmetry directions  $\bar{\Gamma}X$  and  $\bar{\Gamma}M$  of the two-dimensional BZ.

BL's. Therefore, measurable physical properties depending on level energy, as direct optical transitions, will show a dependence on the SL periods different from those presented by the corresponding BL's.

For spin-down electrons the general picture is analogous to that described above, although due to the large increase in the number of bands the image is more entangled. Figures 6 and 7 display the spin-down electronic dispersion relations for the  $\text{Ni}_4\text{Co}_5$  SL and BL. A detailed analysis shows the same kind of behavior as that for spin-up electrons. Anti-

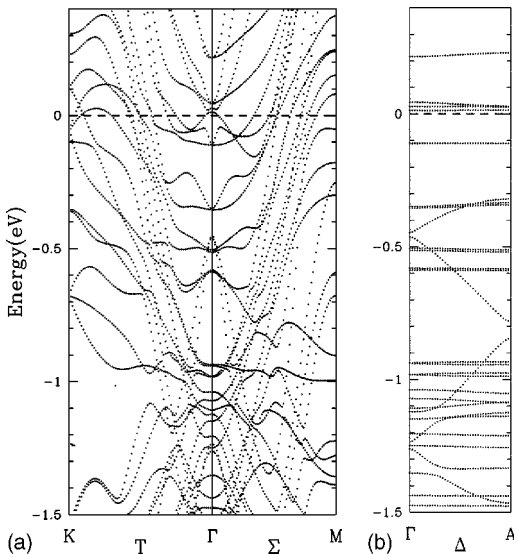


FIG. 6. Same as Fig. 1 for spin-down polarized states.

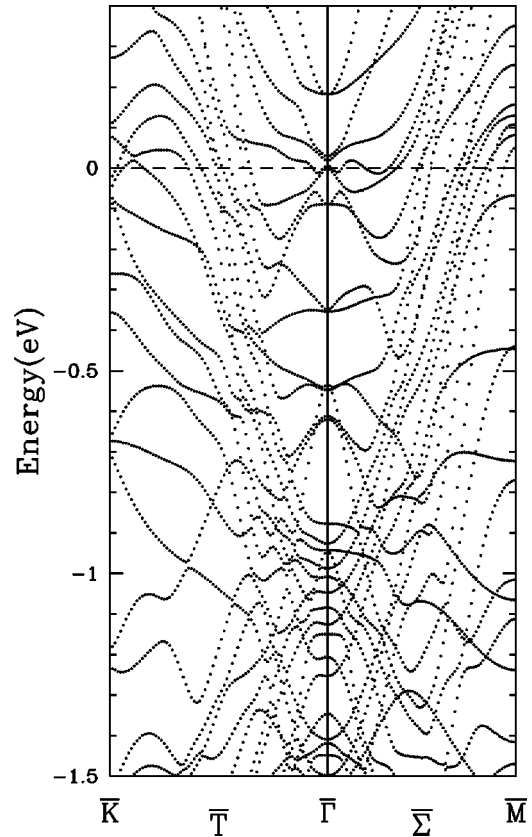


FIG. 7. Same as Fig. 2 for spin-down polarized states.

crossings in the  $T$  direction are clearly identified, being larger in the BL dispersion relation. Furthermore, BL energy levels with a predominant  $d$ -like character are located approximately at the middle of the SL  $\Delta$  bands for both spin-up and spin-down electrons. This is clearly inferred from Fig. 8, where the orbital decomposed LDOS of spin-up electrons as a function of energy is represented at the  $\Gamma$  point for the  $\text{Ni}_4\text{Co}_5$  BL and at  $k=0.5$  in the  $\Delta$  direction for the corresponding SL. The small energy differences between SL and BL states are due to the different boundary conditions of the nine-layer slab unit block. However, the energy position of SL and BL states with a predominant  $sp$ -like orbital character is dissimilar, as can be seen in Fig. 8. The different behavior of  $sp$  and  $d$ -like electrons is spin-independent.

The interchange of the number of Ni and Co layers for a fixed SL period does not alter noticeably the electronic structure of spin-up  $\text{Ni}_5\text{Co}_4$  SL and BL electrons. The distinction is almost negligible. Both  $\text{Ni}_4\text{Co}_5$  and  $\text{Ni}_5\text{Co}_4$  structures have the same number of bands and similar dispersion in the energy region around the Fermi level for the high-symmetry directions. For spin-down electrons there are some (although small) differences, due to the different interaction of the Ni and Co  $d$  bands with the  $sp$  free-electron bands. Nevertheless, the discrepancies are small and almost confined to the crossing or anticrossing of specific bands. This characteristic has its origin in the similar band structure, close to the Fermi level, of Ni and Co fcc metals at the  $L$  point. Around  $E_F$  the SL subbands and the BL energy levels come from the  $L_2'$  and  $L_3$  Ni and Co bulk levels, which are at very close

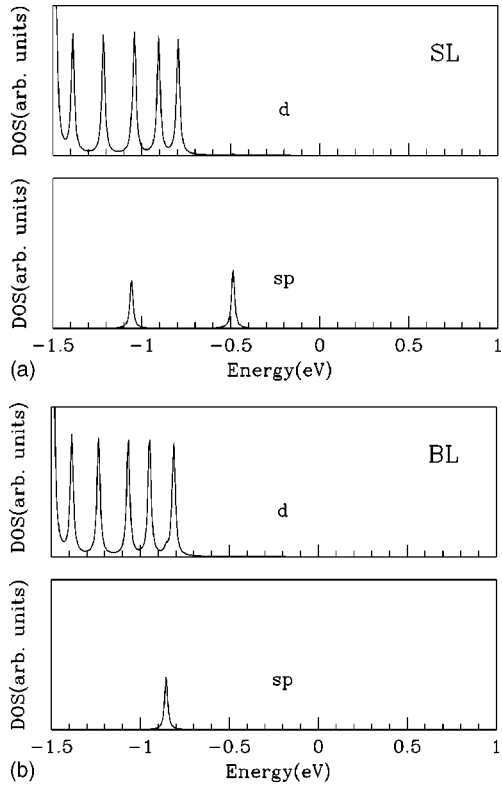


FIG. 8. Spin-up polarized orbital-decomposed local DOS: (a) for the  $\text{Ni}_4\text{Co}_5$  BL at  $\Gamma$ ; (b) for the  $\text{Ni}_4\text{Co}_5$  SL at  $k=0.5$  in the  $\Delta$  direction.

energies.<sup>19</sup> The similar bulk structure gives rise to a low-energy barrier at the interface, which in turn infers a peculiar property to most of the  $d$ -like electronic states close to the Fermi level of  $\text{Ni}_n\text{Co}_m$  SL's and BL's. In spite of the well-known large spatial localization of  $d$  states, the  $d$ -derived SL and BL bands are almost delocalized in real space, as shown in Figs. 9 and 10, which display the spatial distribution of the spectral strength for spin-down states close to  $E_F$  for  $\text{Ni}_4\text{Co}_5$  and  $\text{Ni}_5\text{Co}_4$  structures, respectively. The wave functions are

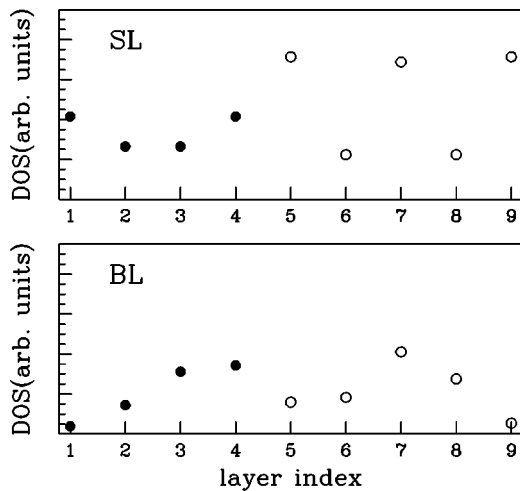


FIG. 9. Spatial distribution of the spectral strength for spin-down states at the  $E_F$  region for both  $\text{Ni}_4\text{Co}_5$  SL and BL.

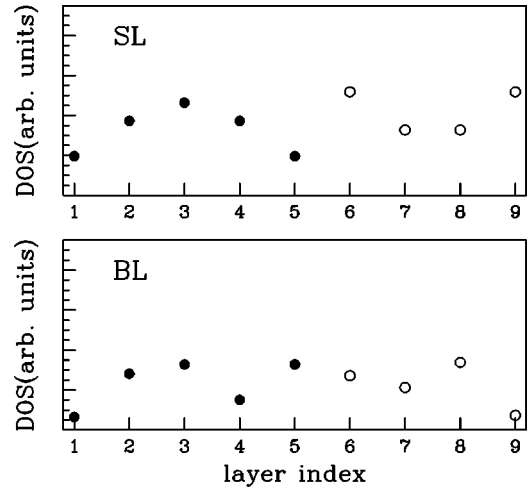


FIG. 10. Spatial distribution of the spectral strength for spin-down states at the  $E_F$  region for both  $\text{Ni}_5\text{Co}_4$  SL and BL.

not confined to either the Ni or the Co slab. This property is shown by both SL's and BL's. In fact, the wave function corresponds to quantization of bulk standing waves with a well-defined number of maxima. In Fig. 9 two states with very close energies but different origin are represented, while Fig. 10 displays SL and BL states with the same number of maxima in the wave function; due to the asymmetry of the potential barrier, the bilayer layer DOS presents an asymmetric distribution with respect to the Ni and Co slab center.

Summarizing, although electron mixing and hybridization control the electronic structures of SL's and BL's, the actual SL dispersion relations are dominated by the translational invariance in the SL growth direction, while those corresponding to BL reflects the lowering of symmetry. Then, for a given  $\mathbf{k}$  or for a given energy the Bloch spectral functions are different. As shown in Figs. 9 and 10, almost all ML states correspond to quantum-well-like states with an inhomogeneous probability function along the layers. However, the oscillations flatten out when summing over all the BL and SL BZ's to obtain the total DOS. There is no large deviation of the magnetic moment of the surface and interface layers in both SL's and BL's, with values comparable to those of the corresponding bulk Ni and Co. As was presented in a previous work,<sup>7</sup> the calculated magnetic moments of a single Ni/Co(111) interface formed by two semi-infinite Ni and Co crystals show a small variation, being an increase in Ni and a slight decrease in the Co interface layers. In the aforementioned article, the interface magnetic moments were calculated by a self-consistent iterative procedure. In the present case, although not calculated self-consistently, we do not find a significant charge transfer and the layer-resolved magnetic moments are similar to the bulk values, analogously to those found in the single interface. A bulklike magnetic profile is in good agreement with recent theoretical calculations of the layer-resolved magnetic spin moments of the Ni/Co(111) fcc interface based on the first-principle Green-function method.<sup>6</sup> To our knowledge, there are no experimental results for Ni/Co (111) ML's, but x-ray magnetic circular dichroism experiments on Ni/Co(100) suggest<sup>2,3</sup> a high degree of  $d$ -charge redistribution between Co and Ni  $d$  states.

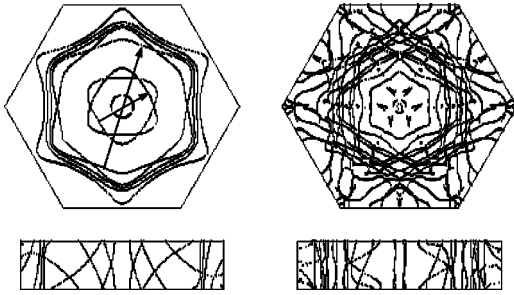


FIG. 11. Spin-up and spin-down Fermi surface cross sections of the  $\text{Ni}_4\text{Co}_5$  SL at the bisector  $k_z=0$  plane and at one of the three reflection planes parallel to the (111) growth direction of the BZ.

Moreover, the change in the  $d$ -state occupancies results in an increased Co magnetic moment and a reduced Ni spin moment at the epitaxially grown Ni/Co interface on a Cu(001) surface. This result contradicts recent band-structure calculations that, analogously to the Ni/Co(111) interface calculation,<sup>6,7</sup> predict a small charge transfer and bulklike magnetic moments.

The discrepancies between SL and BL band structures explained above suggest that the corresponding Fermi surfaces (FS's) may also show a dissimilar structure. Figures 11 and 12 display spin-up and spin-down FS cross sections of the  $\text{Ni}_4\text{Co}_5$  SL and BL, respectively. The bisector  $k_z=0$  plane and one of the three reflection planes parallel to the (111) growth direction are represented for the  $\text{Ni}_4\text{Co}_5$  SL in Fig. 11, while the corresponding 2D FS of the bilayer is presented in Fig. 12. In-plane spin-up SL cross-section and BL spin-up FS's have an analogous multisheet structure from a topological point of view. They are formed by eight distorted circles with full hexagonal symmetry. Nevertheless, the shape of some of the interior SL and BL sheets differs: intersection of adjacent sheets occurs in the SL FS while in the BL the sheets are always separated. In the SL, crossing of sheets is not restricted to the  $k_z=0$  plane; it also appears at different values of  $k_z$ , as shown by the FS cross section in a plane parallel to the SL (111) growth direction. Then, although the number of sheets is the same, SL and BL have a different sheet distribution in  $k$  space. The spin-down FS's also present significant differences, but due to their complexity—the number of sheets increases considerably—it is difficult to isolate the effects. However, as for spin-up electrons, the crossing of sheets is larger in the SL than in the BL Fermi surfaces.

A peculiar Fermi surface characteristic of both SL's and BL's is the strong nesting. Either several sheets nest into each

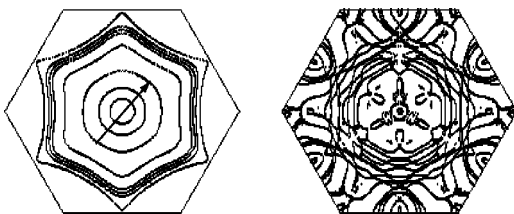


FIG. 12. Spin-up and spin-down 2D Fermi surfaces of the  $\text{Ni}_4\text{Co}_5$  BL.

other or different portions of a particular sheet nest. In general, nesting vectors couple FS points on the same sheet in the BL and on different sheets in the SL. Thus, nesting vectors are different for SL's and BL's formed with the same unit block. This introduces an important difference, since screening anomalies or dynamical coupling between electronic vibrational or magnetic degrees of freedom may be changed just by introducing the superperiodicity. Two and one representative nesting vectors are shown in the spin-up FS's in Figs. 11 and 12, respectively. In the BL the nesting vector couples two points on the same sheet. Then, they would give rise to screening anomalies similar to those occurring at  $2k_F$  in bulk materials. As it is clear from Fig. 12, there are as many nesting vectors of this kind as the number of sheets. In the SL, although there are some nesting vectors coupling points in the same sheet, most of them couple points belonging to different sheets of the FS, as those shown in Fig. 11. Therefore, they could couple low-energy excitations—with a momentum spanning these FS points—to the electron-hole continuum. In particular, this would yield dynamical coupling between electronic and magnetic degrees of freedom and may result in electronic instabilities, with the FS driving long-range effects in the spin-wave spectrum. The differences between SL and BL FS may also result in different transport coefficients. In fact, transport properties depend not only on the ML electronic structure, but also on the electronic coupling of the ML and the metallic leads. Thus, the contact resistance may depend on the superperiodicity. We have presented a qualitative description of the BL and SL electronic structure. The calculation method is particularly suitable, since multiple scattering and boundary conditions are treated exactly within the model Hamiltonian employed. Finite-size effects in measurable physical quantities should require more precise band-structure calculations.

#### IV. FINAL REMARKS

The electronic properties of  $\text{Ni}_n\text{Co}_m$  bilayers and the corresponding superlattices, formed by a periodical repetition of the bilayer unit block, show common characteristics such as the presence of highly hybridized  $sp-d$  states at the Fermi level, the existence of strongly nested multisheet Fermi surfaces, and the occurrence of spatially extended states with a predominant  $d$ -like orbital component. The extended character of  $d$ -like states at the Fermi level may have important implications in the transport properties of  $\text{Ni}_n\text{Co}_m$  heterostructures, particularly in the magnetoresistance effect. Since the wave function of  $d$ -derived states is delocalized along the entire  $\text{Ni}_n\text{Co}_m$  unit block and  $d$  states have a large spin polarization, the system may support large spin currents dominated by the  $d$ -band contribution in the heterostructure growth direction. Nevertheless, there are distinct properties due to the periodic SL potential. In fact, SL energy bands are highly degenerate compared to those of the corresponding BL. This results in different energies at a given  $\mathbf{k}_{\parallel}$  for electrons belonging to the same subband; therefore  $\mathbf{k}$ -dependent properties such as optical or electro-optical effects may show finite-size effects. In particular, magnetic or electrical susceptibility as well as electron-vibrational dynamical coupling may depend on the finite or periodic character of the multilayer structure.

## ACKNOWLEDGMENTS

This work has been partially supported by the Spanish Ministry of Ciencia y Tecnología through

DGICYT Projects Nos. BFM2000-1330 and BFM2000-1107 and the Comunidad de Madrid CAM-07N/0092/1998.

- 
- <sup>1</sup>G. H. Daalderop, P. J. Kelly, and F. J. A. den Broeder, *Phys. Rev. Lett.* **68**, 682 (1992).
- <sup>2</sup>P. Srivastava, N. Haack, H. Wende, R. Chauvistré, and K. Baberschke, *Phys. Rev. B* **56**, R4398 (1997).
- <sup>3</sup>P. Srivastava, F. Wilhelm, A. Ney, M. Farle, H. Wende, N. Haack, G. Ceballos, and K. Baberschke, *Phys. Rev. B* **58**, 5701 (1998).
- <sup>4</sup>S. S. Dhesi, H. A. Durr, G. van der Laan, E. Dudzik, and N. B. Brookes, *Phys. Rev. B* **60**, 12 852 (1999).
- <sup>5</sup>S. S. Dhesi, H. A. Durr, E. Dudzik, G. van der Laan, and N. B. Brookes, *Phys. Rev. B* **61**, 6866 (2000).
- <sup>6</sup>A. M. N. Niklasson, B. Johansson, and H. L. Skriver, *Phys. Rev. B* **59**, 6373 (1999).
- <sup>7</sup>A. Ernst, G. van der Laan, W. M. Temmerman, S. S. Dhesi, and Z. Szotek, *Phys. Rev. B* **62**, 9543 (2000).
- <sup>8</sup>O. Hjorstam, J. Trygg, J. M. Wills, B. Johansson, and O. Eriksson, *Phys. Rev. B* **53**, 9204 (1996).
- <sup>9</sup>F. Erler, P. Zahn, and I. Mertig, *Phys. Rev. B* **64**, 094408 (2001).
- <sup>10</sup>J. M. Gallego, D. Lederman, S. Kim, and I. K. Schuller, *Phys. Rev. Lett.* **74**, 4515 (1995).
- <sup>11</sup>D. Lederman, J. M. Gallego, S. Kim, and I. K. Schuller, *J. Magn. Mater.* **183**, 261 (1998).
- <sup>12</sup>M. Weissmann, A. M. Llois, R. Ramirez, and M. Kiwi, *Phys. Rev. B* **54**, 15 335 (1996).
- <sup>13</sup>S. Sanvito, C. J. Lambert, J. H. Jefferson, and A. M. Bratkovsky, *Phys. Rev. B* **59**, 11 936 (1999).
- <sup>14</sup>J. L. Pérez-Díaz, Tesis Doctoral, Universidad Complutense de Madrid, Spain (1995).
- <sup>15</sup>M. C. Muñoz and J. L. Pérez-Díaz, in *2nd International Symposium on Metallic Multilayers*, Cambridge, 1995, Abstract Book, p. 140.
- <sup>16</sup>J. Opitz, P. Zahn, and I. Mertig, *Philos. Mag. B* **78**, 556 (1998).
- <sup>17</sup>M. P. López-Sancho, L. Chico, and M. C. Muñoz, *Phys. Rev. B* **59**, 1232 (1999).
- <sup>18</sup>M. C. Muñoz, V. R. Velasco, and F. García-Moliner, *Phys. Rev. B* **39**, 1786 (1989).
- <sup>19</sup>V. L. Moruzzi, J. F. Janak, and A. R. Williams, *Calculated Electronic Properties of Metals* (Pergamon, New York, 1978).
- <sup>20</sup>D. A. Papaconstantopoulos, *Handbook of the Band Structure of Elemental Solids* (Plenum, New York, 1986).
- <sup>21</sup>C. M. Schneider, P. Schuster, M. Hammond, H. Ebert, J. Noffke, and J. Kirschner, *J. Phys. C* **3**, 4349 (1991).
- <sup>22</sup>G. J. Mankey, R. F. Willis, and F. J. Himpsel, *Phys. Rev. B* **48**, 10 284 (1993).